Realization of conformal doping on multicrystalline silicon solar cells and black silicon solar cells by plasma immersion ion implantation*

Shen Ze-Nan(沈泽南), Xia Yang(夏 洋), Liu Bang-Wu(刘邦武)†,
Liu Jin-Hu(刘金虎), Li Chao-Bo(李超波), and Li Yong-Tao(李勇滔)

Key Laboratory of Microelectronics Devices and Integrated Technology, Institute of Microelectronics, Chinese Academy of Sciences, Beijing 100029, *China*

(Received 5 March 2014; revised manuscript received 29 May 2014; published online 24 September 2014)

Emitted multi-crystalline silicon and black silicon solar cells are conformal doped by ion implantation using the plasma immersion ion implantation (PIII) technique. The non-uniformity of emitter doping is lower than 5%. The secondary ion mass spectrometer profile indicates that the PIII technique obtained 100-nm shallow emitter and the emitter depth could be impelled by furnace annealing to 220 nm and 330 nm at 850 °C with one and two hours, respectively. Furnace annealing at 850 °C could effectively electrically activate the dopants in the silicon. The efficiency of the black silicon solar cell is 14.84% higher than that of the mc-silicon solar cell due to more incident light being absorbed.

Keywords: solar cells, plasma immersion ion implantation, conformal doping, black silicon

PACS: 88.40.H–, 85.40.Ry, 52.77.Dq, 73.63.–b **DOI:** 10.1088/1674-1056/23/11/118801

1. Introduction

The optimization of an emitter is crucial to increasing solar cell efficiencies. Gas diffusion (e.g., $POCl_3$) has been widely used to dope the emitter in the silicon solar cell industry. During the phosphorous thermal doping process, phosphosilicate glass (PSG) is formed on the whole surface of wafers.[1] Furthermore, since the passivation property of the PSG is poor compared with other passivation layers such as SiN_x and SiO_2, the PSG removal process is needed. Ion implantation, compatible with device processes, could be an alternative technique for the thermal doping process. This technique is cost effective because it does not need the removal of by-products such as PSG and the edge isolation process.[2–4] In addition, it is more advantageous in the uniformity, controllability, and reproducibility of doping. Recently, homojunction crystalline silicon solar cells with ion-implantation technology have been demonstrated with conversion efficiencies ranging from 18.73% to 19.1%,[2–4] with a conversion efficiency improvement of at least 0.8% absolute with respect to conversional thermal $POCl_3$-based emitters, and without deepened optimization. Ion implantation could precisely control the implantation direction, which is useful to prepare advanced structure solar cells, such as selective emitter solar cells, interdigitated back contact solar cells, and so on.[5,6] However, ion beam implantation technology with an accelerating power supply and mass analyzer makes the application in solar cells more expensive.[7] Plasma immersion ion implantation (PIII) technology with its simple and robust structure and its ability to implant a high dose on a large substrate in a short time could be economically acceptable and find its place in the solar cells market.[8,9] The cell efficiency of PIII doping on crystalline silicon was improved by 0.8% absolute.[7] Unlike the beam-line implantation technique, the PIII process is not dependent on the implanted surface and could realize conformal doping. In this paper, we study the PIII doping on multicrystalline silicon and black silicon solar cells. We discuss the influence of PIII doping dose and annealing condition on the performance of multicrystalline silicon and black silicon solar cells.

2. Experimental

In this study, P-type multicrystalline silicon (mc-Si) was used as the initial substrate with an area of 156 mm×156 mm, resistivity of 1–3 Ω·cm, and thickness of 200 μ·m. Before mc-Si was applied to be implanted to form the emitter, the surface contamination was removed by etching in a H_2O:HF (10:1) solution. The black silicon was produced on the mc-Si by plasma immersion ion implantation (PIII) texturing.[10] The PIII technique was composed of a vacuum chamber containing a plasma source, a gas inlet, and a conducting substrate with a rectangular high-voltage negative pulse. When the high-voltage negative pulse was applied, an ion sheath was formed around the wafer. Then, doping ions were accelerated toward the substrate surface, where they were implanted.

To form the N emitter region, a PH_3 gas as the phosphorus source was used. PH_3 gas was ionized by inductively coupled plasma (ICP), and P^*, PH^*, PH_2^*, and H^* were implanted into the substrate with a negative pulse voltage of 2 kV, a pulse frequency of 100 Hz, and a pulse duration of 50 μs. The implan-

*Project supported by the National Natural Science Foundation of China (Grant Nos. 61106060 and 61274059) and the National High Technology Research and Development Program of China (Grant No. 2012AA052401).

†Corresponding author. E-mail: liubangwu@ime.ac.cn

© 2014 Chinese Physical Society and IOP Publishing Ltd

tation dose is mainly controlled by the implantation time, ICP radio frequency power, and PH_3 flow. In order to reduce the ion collision frequency and decrease implantation energy loss, the chamber pressure should be lower than 1 Pa. Furthermore, to active the dopant electroactivation and repair the damage, we used rapid thermal annealing (RTA) (1100 °C, 20 s) and furnace annealing (850 °C, 1 or 2 hours).

The non-uniformity of doping was tested by a four-point probe with the mapping model. A secondary ion mass spectrometer (SIMS) was used to detect the profile of implantation dopants and ion dose. The recombination of emitter can be characterized by minority carrier lifetime with the microwave detected photoconductive decay (μ-PCD) method.[11] The solar cell performance was tested under an AM1.5G solar simulator with a light intensity of 100 mW/cm^2. Quantum efficiencies of solar cells were measured by the QEX7 measurement system.[12]

3. Results and discussion

3.1. Uniformity of PIII doping technology

Figures 1(a) and 1(b) present the schematic illustration of PIII and the corresponding distribution of ion density. The distribution of plasma is simulated by CFD software with the finite volume method. To simplify the cylindrical symmetry chamber structure, we simulate the ion density distribution in two dimensions. Figure 1(c) shows that the ion density in the middle of the substrate is higher than that at the sides, but the non-uniformity is lower than 3% in theory analysis. Figure 1(d) illustrates the sheet resistance mapping of the PIII. The experimental result indicates that the non-uniformity is less than 5%, which is acceptable for mc-Si solar cell application.

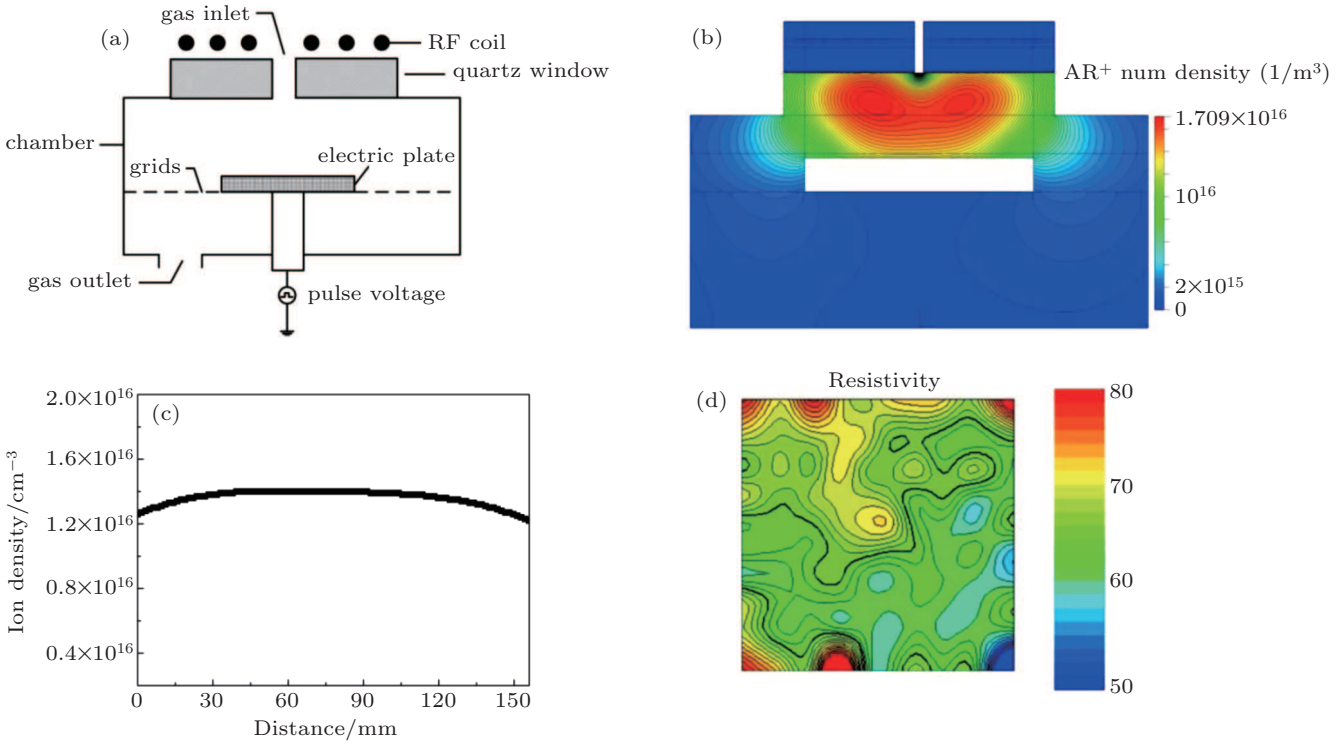


Fig. 1. (color online) (a) Schematic illustration of PIII equipment; (b) ion density distribution in chamber simulated by CFD; (c) distribution of ion density upon 1-mm substrate; and (d) sheet resistance mapping showing a non-uniformity σ/μ (standard deviation/average) of $< 5\%$.

3.2. Emitter optimization

The phosphorous implanted area in the silicon is partially or totally amorphised.[13] To recrystallize silicon and activate the dopants, the wafers are annealed by RTA or furnace annealing technology, resulting in a redistribution of the dopant profile and impelling the depth of the PN junction. The sheet resistance represents the electronic activation rate of the phosphorus implanted in silicon. Figure 2 presents the phosphorus implanted profiles of the as-implanted, the various annealing conditions and the oxygen intensity of the as-implanted in the substrate measured by the SIMS. The implanted phosphorus in the silicon is present in three forms: ionized phosphorus (in the substitute position), mobile phosphorus (in the interstitial position), and in the form of aggregates (percolation network). The ionized phosphorus acts as the electronical activity and

the electron carrier density is defined as follows:[14]

$$n_e = 9.2 \times 10^{21} \exp(-0.33/kT).$$

In this experiment, the annealing condition is 1100 °C RTA and 850 °C furnace annealing. The calculated electron carrier density at 1100 °C and 850 °C is 5.7×10^{20} and 3.7×10^{20} cm^{-3}, respectively. For the furnace annealing condition, the phosphorus atom diffuses into the deeper silicon area with one or two hours annealing, and consequently, the surface phosphorus concentration decreases to the electronic active concentration. However, for the 1100 °C RTA process, the surface phosphorus concentration exceeds the electron activation concentration due to the deactivation during cooling.[14] The major advantage of the PIII technique is high dose and low energy, which is suitable for a shallow junction of solar cells. The as-implantation profile shows that phosphorous dopants accumulate at the surface area and the concentration exceeds 1×10^{21} cm^{-3}. The PN junction depth is about 100 nm at 1×10^{16} cm^{-3} (corresponding to the resistivity of p-type crystalline silicon, i.e., 1.5 Ω·cm). After the annealing process at 850 °C for an hour and two hours, the profiles show an acceleration of diffusion with time, leading to less concentration at the surface and deeper profiles, respectively. The junction depth with an hour and two hours annealing processes are about 220 nm at 1×10^{16} cm^{-3} and 330 nm at 1×10^{16} cm^{-3}, respectively. In view of the screen print and firing process, the junction depth is always at 300–500 nm. The furnace annealing condition at 850 °C for two hours is needed. After RTA at 1100 °C for 20 s, the phosphorus profile is more abrupt at near surface area.

During the PIII process, at least three simultaneous events take place, namely, implantation of ions into the substrate, etching the silicon surface by sputtering, and formation of an oxide layer.[15] According to the as-implanted oxygen intensity profile, the oxide layer thickness is calculated to be about 5.7 nm. The oxide layer is thicker than the native oxide layer, which may be caused by the etching quartz window of the processing chamber during implantation.[15] There are two peak concentrations in the as-implanted phosphorus profile. The peak in the oxide layer corresponds to the implantation depth of 2-keV PIII implantation energy. The second phosphorus peak at the SiO_2/Si interface is due to an accumulation effect of the interface defect. The stopping and range of ions in the matter (SIRM) software are applied to analyze the ion interaction with silicon. The simulation results show that 2-keV beam-line ion implantation energy obtains an implantation depth (peak position) of 5.3 nm. Considering the dispersity of the PIII implantation energy, the ionized phosphorus obtains a maximum of 2 keV. The implantation energy of phosphorus varies from 0 to 2 keV. This reduces the ion range of implantation atom and meanwhile makes the doping depth narrower.

The advantages of the PIII technique are the high dose and low damage. In this experiment, the dose of PIII doping is around 2×10^{15} cm^2 and the implantation depth is about 23 nm at 1×10^{18} cm^2. In contrast, if the ion implantation technique obtains the same implantation dose, it should power up the implantation energy above 10 kV. Consequently, the implantation depth and implantation damage area get deeper. The amorphous surface layer introduced by the PIII doping is accumulated near the surface while the ion implantation is extended into the bulk. We could deduce that the substrate capped with the SiO_2 layer is good for implantation. Because the damage layer resides in the SiO_2 layer, it could be etched away by the HF solution and consequently improve the surface electrical properties of the implanted solar cell.

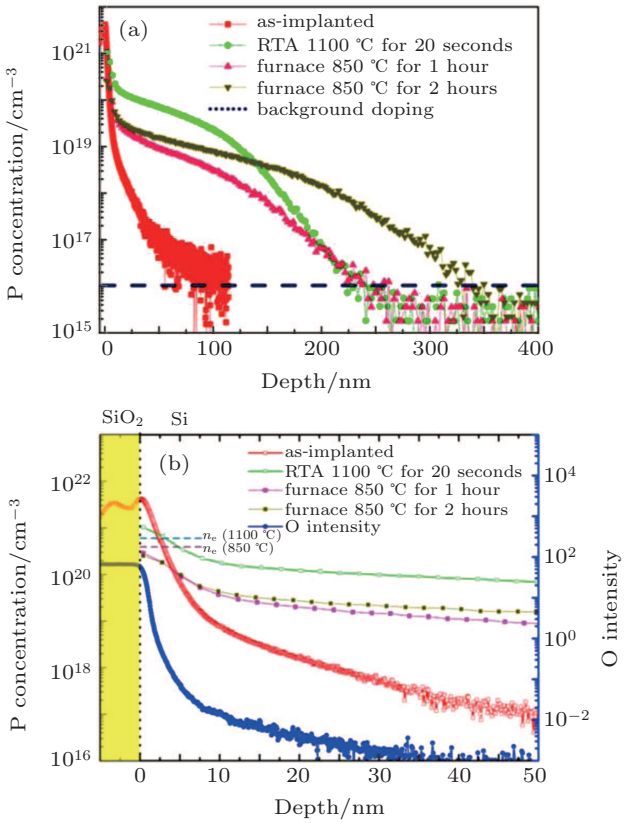


Fig. 2. (color online) (a) SIMS profiles of phosphorus-implanted emitters as a function of annealing conditions. (b) Detail information of SIMS profiles of phosphorus-implanted near the surface.

To investigate the quality of an emitter formed by PIII phosphorus doping, minority carrier lifetime is applied to characterize the electrical property. Figure 3 presents the lifetime as a function of the implantation and annealing process. To activate the phosphorus activity, we use the RTA process and furnace annealing process. After the RTA process, the lifetime decreases dramatically to 0.1–0.4 μs. This could be attributed to metal contamination.[16,17] RTA with temperature higher than 900 °C redistributes and activates

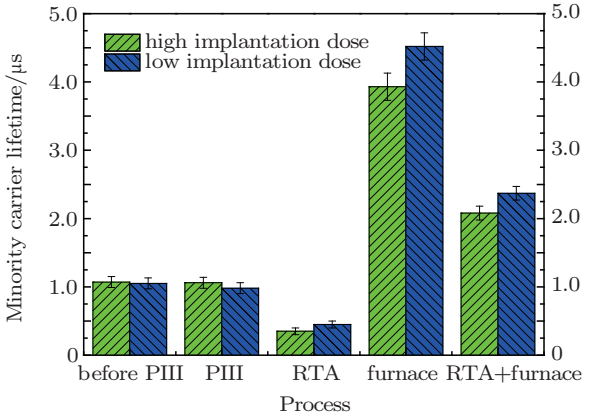


Fig. 3. (color online) Minority carrier lifetime varies with the wafer process. After the PIII process, the wafer was sent to rapid thermal annealing or furnace annealing. The furnace annealing increases the lifetime and the RTA process reduces the lifetime.

the impurity metal in silicon.[18] High temperature processing that influences the minority carrier diffusion length, since impurities are highly mobile at elevated temperatures.[19] The furnace process at 850 °C increases the lifetime up to 4 μs. During the 2 hours furnace process, the oxide layer is formed which is good for passivation and consequently improves the lifetime. The lifetime of a wafer with a high implantation dose is lower than that of one with a low implantation dose. This indicates that the inactivation of implantation dopant has some relation with the implantation dose.

3.3. PIII conformal doping

Figures 4(a) and 4(b) present the scanning electron microscope (SEM) pictures of black silicon in side view and top view. The structure size of black silicon is about several hundred nanometers with sharp morphology. We establish a schematic diagram to illustrate the difference of the implantation process in beam-line implantation (Fig. 4(c)) and the PIII technique (Fig. 4(d)). The ions ejected from the beam-line implanter are vertical to the wafer surface, but have a tilt angle to the surface of the black silicon layer. However, the ions produced by PIII surround the surface morphology and are vertical to the black silicon layer. With every single pulse voltage, the ions are conformally implanted into the silicon.

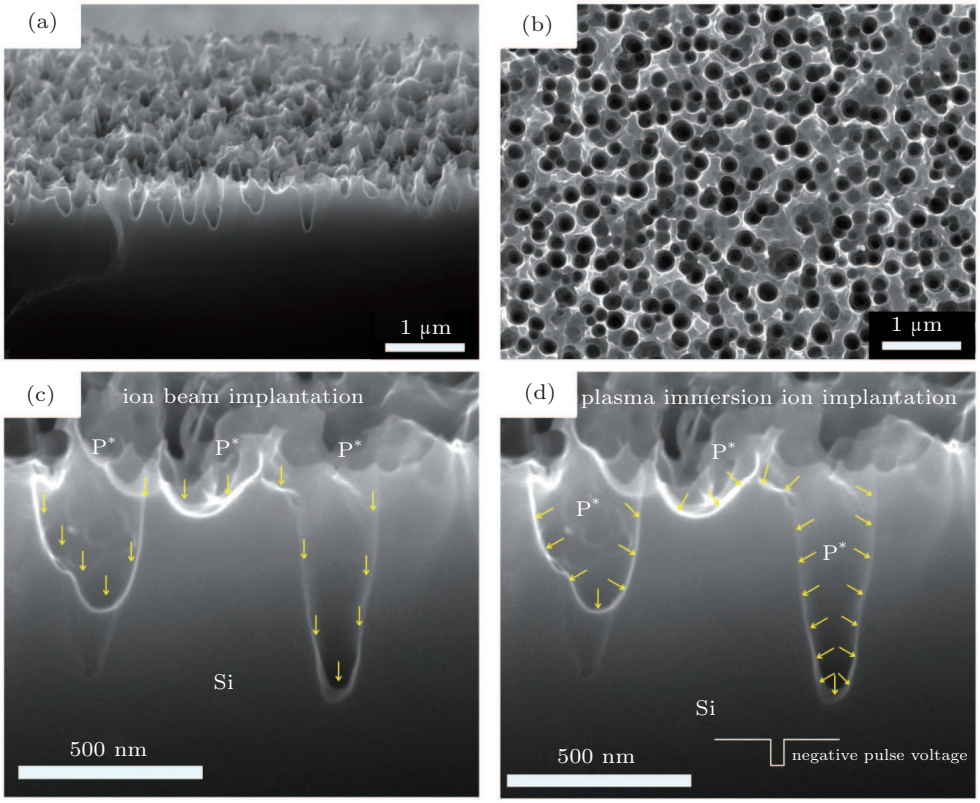


Fig. 4. (color online) SEM picture of black silicon with side view (a) and top view (b). Phosphorus implantation model of beam-line ion implanter (c) and PIII (d) on the black silicon surface. PIII could realize conformal implantation on black silicon.

3.4. Performance of solar cells

The performance of mc-Si solar cells and black-Si solar cells are listed in Table 1. The conversion efficiency of the black-Si solar cell is 14.84%, higher than that of the mc-Si solar cell. It could be attributed to low reflectivity and produce more photo-induced carriers as the short circuit current gains more. This can also be approved from the external quantum efficiency (EQE) of solar cells. Figure 5 presents the EQE of

mc-Si solar cell and black-Si solar cell. Due to the enlarged surface area of black silicon, it increases the surface recombination. Meanwhile, the nanostructure of black silicon absorbs much more incident light, resulting in low reflectivity. However, the EQE at shortwave response reduces due to high surface recombination. The long-wave response increases due to low reflectivity. The leak current of PIII solar cells goes beyond by one order of magnitude. The metal defects in the mc silicon and black silicon becomes a leakage path rather than recombination centers.[20] The increase in J_{rev} for the phosphorus emitters is not due to the recombination in the emitter, but the effect of the bulk lifetime.[13] The ion implantation damage at the surface of silicon could be repaired with suitable furnace annealing, but the defect in the silicon still remains. The intrinsic defect limits the majority lifetime and cell efficiency.[21] The conversion efficiencies of solar cells with the PIII doping technique, however, are lower than those with the thermal doping process. To further increase the cell efficiency of implantation doping, one should have a substrate with a better intrinsic lifetime.

Table 1. Electrical parameters of mc-Si solar cells and black-Si solar cells.

Cell type	Eff/%	V_{oc}/V	J_{sc}/mA·cm^{-2}	FF	R_s/Ω	R_{sh}/Ω	J_{rev}/mA·cm^2
mc-Si	13.56	0.575	30.70	0.768	0.0066	25.35	13.2
Black-Si	14.84	0.594	32.26	0.775	0.0061	34.22	12.7
mc-Si (thermal doping)	17.21	0.625	35.54	0.775	0.0053	4.2	1.2

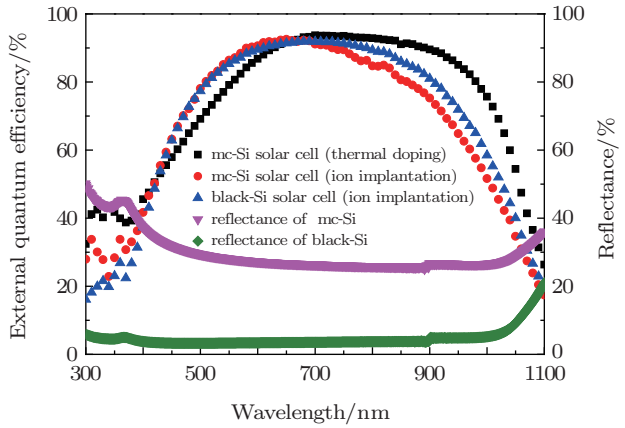


Fig. 5. (color online) External quantum efficiency spectra of solar cells with the reflectance of mc-Si and black-Si solar cell with thermal doping (reference cell) has better performance at the short-wave response and long-wave response. A black silicon solar cell with ion implantation obtaining a rougher surface reduces the short-wave response, but increase the long-wave response compared with the mc-silicon solar cell.

4. Conclusion

In this paper, we discussed the plasma immersion ion implantation application on mc-Si and black silicon solar cells. PIII could realize conformal doping on mc-Si and black silicon, and the non-uniformity of implantation is lower than 5%, which is suitable for industry mass production. Furnace annealing at 850 °C could effectively activate the dopant implanted in the silicon and impels the emitter depth to 220 nm and 330 nm with 1 hour and 2 hours, respectively. Solar cell performance indicates that the intrinsic defect in mc-silicon becomes the leakage path and reduces the quantum efficiency. To further improve the electrical performance of PIII, doping solar cell should use a low intrinsic defect substrate or be incorporated with an effective gettering method.

References

[1] Bazer-Bachi B, Fourmond E, Papet P, Bounaas L, Nichiporuk O, Le Quang N and Lemiti M 2012 *Sol. Energy Mater. Sol. Cells* **105** 137

[2] Rohatgi A, Meier D L, McPherson B, Ok Y W, Upadhyaya A D, Lai J H and Zimbardi F 2012 *Energy Procedia* **15** 10

[3] Lanterne A, Gall S, Manuel S, Monna R, Ramappa D, Yuan M, Rivalin P and Tauzin A 2012 *Energy Procedia* **27** 580

[4] Hieslmair H, Mandrell L, Latchford I, Chun M, Sullivan J and Adibi B 2012 *Energy Procedia* **27** 122

[5] Bateman N, Sullivan P, Reichel C, Benick J and Hermle M 2011 *Energy Procedia* **8** 509

[6] Jeon M, Lee J, Kim S, Lee W and Cho E 2011 *Mater. Sci. Eng. B* **176** 1285

[7] Perchec J L, Lanterne A, Michel T, Gall S, Monna R, Torregrosa F and Roux L 2013 *Energy Procedia* **33** 18

[8] Torregrosa F, Laviron C, Faik H, Barakel D, Milesi F and Beccaccia S 2004 *Surf. Coat. Technol.* **186** 93

[9] Vervisch V, Barakel D, Torregrosa F, Ottaviani L and Pasquinelli M 2006 *AIP Conf. Proc.* **1** 253

[10] Xia Y, Liu B W, Liu J, Shen Z N and Li C B 2011 *Sol. Energy* **7** 1574

[11] Zhang X R, Gao C M, Zhou Y and Wang Z P 2011 *Chin. Phys. B* **20** 068105

[12] Zhang L, Shen H L, Yue Z H, Jiang F, Wu T R and Pan Y Y 2013 *Chin. Phys. B* **22** 016803

[13] Boo H, Lee J H, Kang M G, Lee K, Kim S, Hwang H C, Hwang W J, Kang H O, Park S, Tark S J and Kim D 2012 *Int. J. Photoenergy* **2012**

[14] Solmi S, Parisini A, Angelucci R, Armigliato A, Nobili D and Moro L 1996 *Phys. Rev. B* **12** 7836

[15] Shaaban E R, Lohner T, Pinter I, Petrik P, Khanh N Q, Horvath Z E and Gyulai J 2003 *Vacuum* **1** 27

[16] Macdonald D and Geerligs L J 2004 *Appl. Phys. Lett.* **18** 4061

[17] Vähänissi V, Haarahiltunen A, Talvitie H, Yli-Koski M and Savin H 2013 *Prog. Photov.* **5** 1127

[18] Prucnal S, Abendroth B, Krockert K, König K, Henke D, Kolitsch A, Moller H J and Skorupa W 2012 *J. Appl. Phys.* **12** 123104

[19] Kwon T Y, Yang D H, Ju M K, Jung W W, Kim S Y, Lee Y W, Gong D Y and Yi J 2011 *Sol. Energy Mater. Sol. Cells* **1** 14

[20] Peaker A R, Markevich V P, Hamilton B, Parada G, Dudas A, Pap A, Don E, Lim B, Schmidt J, Yu L, Yoon Y and Rozgonyi G 2012 *Phys. Status. Solidi. (a)* **10** 1884

[21] Taishi T, Hoshikawa T, Yamatani M, Shirasawa K, Huang X, Uda S and Hoshikawa K 2007 *J. Cryst. Growth* **2** 452